Journal Name

Dynamic Article Links ►

Cite this: DOI: 10.1039/c0xx00000x

www.rsc.org/xxxxxx

ARTICLE TYPE

On the intrinsic photophysics of indigo: A time-resolved photoelectron spectroscopy study of the indigo carmine dianion

Adam S. Chatterley,[a,b] Daniel A. Horke[a] and Jan R. R. Verlet[a]*

Received (in XXX, XXX) Xth XXXXXXXXX 20XX, Accepted Xth XXXXXXXXX 20XX

DOI: 10.1039/b000000x

The intrinsic photophysics of indigo have been studied using gas-phase time-resolved photoelectron imaging of the indigo carmine dianion (InC^{2-}). The action spectrum reveals that the gas-phase absorption spectrum arsing from the $S_1 \leftarrow S_0$ transition in InC^{2-} has a similar solvent shift to that of neutral indigo. Femtosecond spectroscopy shows that the S_1 state decays on a 1.4 ps timescale. Through isotopic substitution, the primary mechanism on the S_1 excited state can be assigned to an intra-molecular proton transfer, which is the same as that that has been observed in solution. However, the excited state lifetime is significantly shorter in vacuum. These similarities and differences are discussed in terms of recent theoretical investigations of the S_1 excited state of indigo.

Introduction

The organic dye, indigo (Fig. 1(a)), and its ring substituted derivatives have been used since ancient times as a distinctive blue stain in applications ranging from Egyptian mummies, to the blue 'war paint' of Celtic warriors and to modern day denim jeans.[1, 2] Historically, the dye was extracted from natural sources, such as the leaves of the *indigofera tinctoria* plant. Over a century ago, however, Adolf von Baeyer successfully synthesised indigo, for which he received the 1905 Nobel Price. Since then, the synthetic route has been extensively used and currently well over 10,000 tons of indigo are produced globally each year.

The reason for the sustained importance of indigo as a dye is not solely due to its striking blue colour, but more importantly because of its resistance to fading after prolonged exposure to light. The blue colour of indigo arises from the strong $S_1 \leftarrow S_0$ transition centred around 600 nm. However, the origin of the photo-resistivity of indigo is more intricate and has been extensively studied. In general, photo-resistive chromophores are a topic of great interest and have, for example, been linked with the survival of primordial organisms on early Earth.[3-5] The photo-resistive properties are related to the excited state dynamics of the chromophore and here we present a direct study of the S_1 dynamics of a disulfonated derivative, indigo carmine (InC^{2-}, Fig. 1(b)), using time-resolved photoelectron spectroscopy.

The luminescent properties of indigo provide clear evidence for its photo-resistance. In dimethylformamide (DMF) solution, the fluorescent quantum yield of indigo is $\Phi_F = 0.0023$, while for InC, it is even lower at $\Phi_F = 0.0015$, despite the large absorption cross section, $\sigma = 3.1 \times 10^{-17}$ cm^2.[6] Hence, a very efficient non-radiative process is operative that effectively out-competes radiative decay. Intersystem crossing has been determined to be almost entirely inactive, while internal conversion accounts for >99% of the

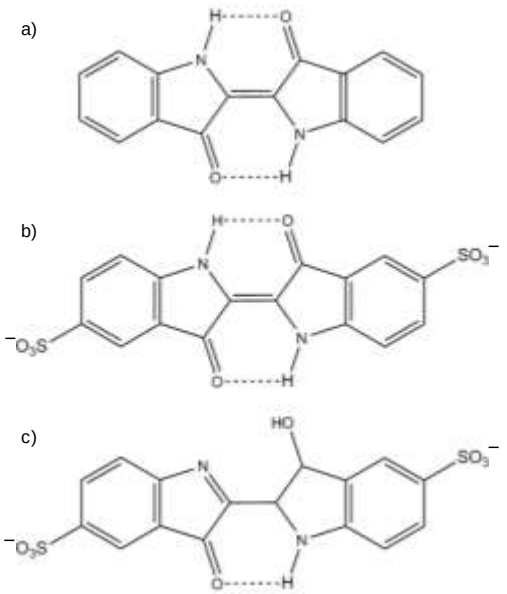

Fig. 1 Molecular structures of a) indigo, b) indigo carmine dianion (InC^{2-}) and c) InC^{2-} in the mono-enol form following excited state single proton transfer

relaxation from the S_1 in indigo and its derivatives.[7] The S_1 lifetime has been determined to be on the order of tens or hundreds of picoseconds, dependent on the specific indigo derivative and the solvent. The reduced (leuco) form of indigo on the other hand has a much longer lived S_1 state, indicating that the keto structure is central to the photo-stability of indigo.[7]

Because of the inherent photo-resistance of indigo, its underlying molecular mechanism has been topical. There are three possible intra-molecular mechanisms that can lead to the rapid internal conversion. Firstly, *trans* → *cis* isomerisation around the central C=C bond can occur. The $S_1 \leftarrow S_0$ transition

corresponds to the promotion of an electron from a π to a π* orbital, which leads to a weakening of the central C=C bond[8, 9] and could in principle result in free rotation around this central carbon bond. Many other dyes with a C=C (stilbenes) or N=N bond (azobenzenes) show considerable *trans-cis* photo-isomerisation yields.[10-12] Indigo, however, does not isomerise,[13] which can be rationalised by the presence of two intra-molecular hydrogen bonds between the C=O and N–H groups in the *trans* form of the molecule (see Fig. 1(a) and (b)). Breaking these hydrogen bonds imposes a large barrier to isomerisation.

The second possible mechanism is excited state intra-molecular proton transfer (ESIPT).[14-16] In this, a proton transfers from an amine group to the adjacent oxygen on the C=O, producing an enol–structure (Fig. 1(c)). The third possible process is a double ESIPT process, in which both hydrogen atoms are transferred in the excited state.

Direct evidence that single ESIPT is operative on the S_1 state was recently provided by Kobayashi *et al*. by means of transient absorption of InC, using sub–5 fs pulses.[17-19] By tracking the temporal evolution of vibronic signatures of InC following photoexcitation, they were able to demonstrate that an alcohol intermediate is formed, while at the same time, the C=O stretch could still be seen. This was taken as direct proof of single ESIPT (Fig. 1(c)). After this intermediate, the system reverts back to the keto-form on the S_1 excited state. The time for a full oscillation of the proton along the ESIPT coordinate was measured to take ~600 fs in methanol. Similar dynamics and timescales were observed in dimethyl sulfoxide (DMSO), indicating that the process is indeed intra-molecular and that the solvent polarity has no significant impact on the ESIPT dynamics. On the other hand, the lifetime of the S_1 excited state is very sensitive to the solvent environment. The fastest excited decay is observed in water, where the S_1 lifetime has been determined to be on average 2.7 ps. In methanol on average it is 23 ps and extends to 100s ps as the solvent polarity is decreased.[20] This suggests that the proton can shuttle back and forth a number of times on the excited state before internal conversion occurs.

Ab initio calculations by Yamazaki *et al*. agree with experiment and indicate that the single ESIPT is the more likely relaxation mechanism.[9] A negligible barrier was calculated for ESIPT on the S_1 potential energy surface and a conical intersection (CI) with the ground state was identified near the enol form that is energetically accessible. A viable CI was also identified along the *trans-cis* isomerisation coordinate; however, a large barrier to isomerisation inhibits this process, in agreement with measurements that indicate that no isomerisation occurs. The possibility of the double ESIPT was also investigated. Although a CI could be identified that would lead to internal conversion, its energy was calculated to be too high to be accessible following excitation to the S_1 state. Hence, it was concluded that single ESIPT was the most likely mechanism by which indigo attains its photo-stability. However, no information about the timescales of the S_1 internal conversion was calculated. Very recently, Cui and Thiel employed nonadiabatic trajectory surface hopping calculations to explore the relaxation mechanism of bispyrroleindigo, a truncated model of indigo.[8] In agreement with the work by Yamazaki *et al*., all population in the excited state was found to decay via near barrierless ESIPT, followed by internal conversion and back-transfer of the proton on the ground state. However, the S_1 lifetime was calculated to be around 700 fs for bispyrroleindigo, significantly shorter than that observed in solution. Moreover, as the calculations assume an isolated system, calculated timescales may be expected to be closer to that in a non-polar solvent and, for indigo, the internal conversion timescales stretches for 100s of ps.

The calculations of Yamazaki *et al*. are considered at the frontier of the size for which excited state surfaces can be calculated at a high level of theory. However, at present, there is no experimental data that allows these calculations to be benchmarked against. Specifically, only studies on solvated indigo derivatives have been performed to date, while the calculations are in vacuum. The same is true for the dynamics study of Cui and Thiel and their extracted timescales do not compare well with those for indigo in aprotic solvents. The current study provides this benchmark highlights the strong influence of the solvent on the excited state lifetimes. Specifically, time-resolved photoelectron spectroscopy[21-23] is employed to study the intrinsic excited state dynamics of the InC^{2-} derivative as a model system of indigo. Moreover, through isotopic substitution, we show conclusively that ESIPT is the primary motion on the excited state and leads to internal conversion. The timescales for decay from the S_1 observed in the gas-phase are significantly faster than all timescales observed in solution and agree moderately well with those calculated by Cui and Thiel. Our results indicate that the solvent plays no constructive role to the photo-stability of indigo, and may in fact impede the relaxation.

Experimental

The experiment has been described in detail elsewhere.[24, 25] Briefly, a 0.5 mM solution of InC sodium salt (Sigma Aldrich) in 20:80 (*v:v*) water:acetonitrile was electrosprayed at –2.5 kV yielding a plume of highly charged droplets containing InC^{2-}. This plume was sampled by a stainless steel transfer capillary and InC^{2-} ions were subsequently accumulated in a home built radio frequency ion trap for ~2 ms and then injected collinearly into a Willey-McLaren time-of-flight mass spectrometer. After field-free flight of 1.3 m, the InC^{2-} ion packet was detected by a pair of multichannel plates (MCPs). The only significant peak in the time-of-flight mass spectrum belonged to InC^{2-} (m/z = 210).

Two lasers sources were employed for photoelectron spectroscopy. The first produced femtosecond pulses to perform time-resolved photoelectron spectroscopy, while a widely tunable nanosecond laser was used to perform absorption action spectroscopy. The femtosecond pulses were derived from a commercial Ti:Sapphire oscillator and regenerative amplifier (Spectra Physics Tsunami and Spitfire XP Pro), delivering 800 nm pulses of 35 fs duration at a repetition rate of 1 kHz and an energy of 2.7 mJ / pulse. Approximately half the fundamental beam is used to pump an optical parametric amplifier (TOPAS, Light Conversion), which generates tunable infrared light. The infrared is mixed with the residual 800 nm beam in a beta-barium borate (BBO) crystal to produce 560 or 530 nm pulses with energies of ~80 μJ / pulse. The remaining half of the fundamental is passed through a BBO to produce pulses at 400 nm with energies ~100 μJ / pulse. A relative delay between the

pulses was introduced using a motorised optical delay line. The two beams were combined collinearly using a dichroic mirror before intersecting the ion packet in the interaction region. The cross correlation of the two pulses was around 130 fs, determined in a thin BBO crystal or by above-threshold photodetachment of iodide. Nanosecond pulses were produced from an optical parametric oscillator (Panther Ex, Continuum), pumped by the 3rd harmonic of an Nd:YAG laser at 10 Hz. The pulses were tunable across the visible and have energies of ~5 mJ / pulse. Both lasers were used unfocussed and laser intensities were on the order of 10^{10} W cm^{-2} and 10^{7} W cm^{-2} for the femtosecond and nanosecond lasers, respectively.

Laser pulses intersected the ion packet perpendicularly in the vacuum chamber and resultant photoelectrons were detected by velocity map imaging (VMI),[24, 26] which collects electrons in a direction orthogonal to both ion and laser beams. The VMI arrangement used electrostatic lenses to focus electrons from the interaction volume to a point on a focal plane determined by the velocity of the electron. At the focal plane, a pair of MCPs coupled to a phosphor screen provided a read-out of the electron position which was captured and accumulated using a CCD. The resultant 2D image was deconvoluted to remove the azimuthal contribution and to produce a central slice through the 3D photoelectron cloud. Deconvolution was performed by the polar onion peeling routine.[27] Radial integration of the deconvoluted image provided the electron velocity, which can be converted to the electron kinetic energy (*eKE*) with the suitable Jacobian and thus provides the photoelectron (PE) spectrum. In addition to energetic information, VMI allows the photoelectron angular distribution (PAD) of the detachment process to be determined. The PADs for this system are of interest because of the multiple charges on InC^{2-}; an electron ejected from the dianion will experience a long-range anisotropic Coulomb barrier that influences the trajectory of the outgoing electron.[28] This will be the focus of a forthcoming publication and is not considered here. PE spectra have been calibrated using the known PE spectrum of I^- at 4.66 eV (266 nm, 3rd harmonic of femtosecond laser). The resolution of the spectrometer is $\Delta eKE/eKE \sim 5\%$.

Results and Analysis

Photoelectron spectroscopy at 4.66 eV

In order to determine the relative energies of the isolated InC^{2-} dianion relative to the anion (radical), the one-colour PE spectrum at 4.66 eV (266 nm) has been acquired with a femtosecond laser and is presented in Fig. 2. Two PE features are observed around *eKE* = 1.2 eV and *eKE* = 1.7 eV. The feature at highest *eKE* can normally be assigned to the direct detachment from the dianion ground state to the ground state of the anion: $InC^{2-}(S_0) + h\nu \rightarrow InC^{-}(D_0) + e^{-}$. From this, the vertical detachment energy of InC^{2-} is estimated to be 3.0 eV. The adiabatic energy is commonly determined by considering the extrapolation of the steepest onset to the *eKE* axis, which for InC^{2-} gives an adiabatic binding energy of ~ 2.5 eV. The feature observed at *eKE* = 1.2 eV suggests that an excited state in the radical anion is accessed upon photodetachment. The energy separation between the two PE peaks is 0.5 eV and it is tempting to equate this with the energy difference between the ground and first excited state in the radical anion. However, the sharp cut-off of PE signal at lower *eKE* suggests that perhaps the entire feature has not been observed.

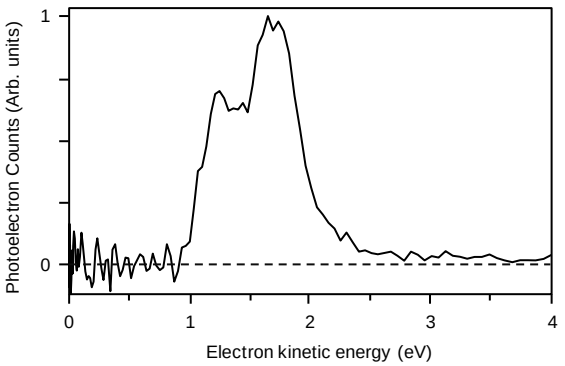

Fig. 2 Photoelectron spectrum of InC^{2-} taken at 4.66 eV (266 nm). A sharp cut-off is observed at low electron kinetic energy (*eKE*), arising from the repulsive Coulomb barrier. The feature at *eKE* = 1.7 eV is assigned to detachment to the ground state of the radical InC^{-} anion.

The appearance of cut-offs in the PE spectra at low *eKE* is a common feature in polyanions. Photoelectrons can only escape from the dianion if the electron has sufficient energy to overcome the repulsive Coulomb barrier (RCB) that arises from the long-range Coulomb repulsion between the outgoing electron and the remaining anion.[29, 30] Below the RCB, photoelectrons can only escape through tunnelling, despite the fact that their kinetic energy is above the $InC^{-}(D_0) + e^{-}$ asymptote.[31] In the present case, the S_1 is lower in energy than this asymptote and no tunnelling feature is observed. The photoelectron cut-off provides a direct measure of the height of the RCB. For InC^{2-}, the RCB height is 1.1 eV as evidenced by the steep rise in photoelectron signal in Fig. 2. In a forthcoming article, the details of the photoelectron imaging and differences between nanosecond and femtosecond photoelectron spectra will be discussed. For the present discussion however, the conclusions from that study have no bearing on the results presented here.

To confirm the relative energies determined from the 4.66 eV PE spectrum, *ab initio* calculations have been performed using density functional theory. All calculations were done at the B3LYP/6-311++G** level of theory using the Gaussian09 package.[32] The adiabatic detachment energy is defined as the difference in energy between the ground state of InC^{2-} and InC^{-} in their respectively optimised geometry and is found to be 2.57 eV (excluding zero-point energies). This is in excellent agreement with the extrapolated 2.5 eV from the PE spectrum. The vertical detachment energy, defined as the energy difference between InC^{2-} and InC^{-} in the dianion geometry, was calculated to be 2.61 eV. This is lower than the measured vertical detachment of 3.0 eV. This discrepancy could be attributed to the finite temperature of InC^{2-} in the current experiment ($T \sim 300$ K) or the fact that the observed spectral maximum does not necessarily coincide with the vertical detachment energy (which often becomes more pronounced with temperature). Nevertheless, the calculated values provide sufficient confidence that the assignment of the energy levels of InC^{2-} is correct. The intrinsic energy level diagram of InC^{2-} is shown in Fig. 3 including various excitation and detachment schemes used for time-and frequency-resolved PE spectroscopy.

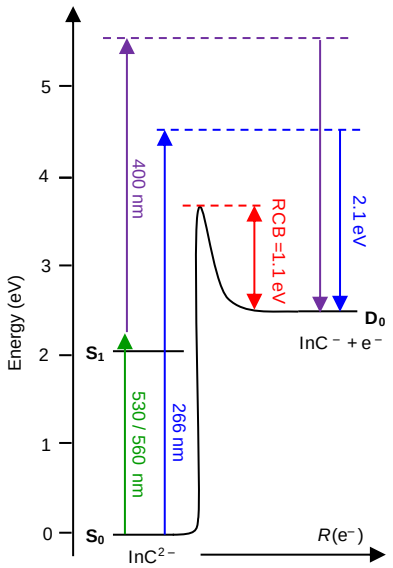

Fig. 3 Energy levels and excitation scheme employed for InC^{2-}. Photoelectron spectra have been taken with 4.66 eV (Fig. 2), leading to direct detachment to the D_0. In pump-probe experiments, a pump at 2.21 eV or 2.33 eV was used while a probe at 3.1 eV was employed to detach from the S_1 state.

Absorption (action) spectrum

Direct photodetachment is only possible for photons with energy above ~ 3.6 eV (λ < 340 nm). Below this energy, PE emission can still be observed due to the resonance enhancement via the $S_1 \leftarrow S_0$ transition of InC^{2-} and the total PE yield measured as a function of photon energy can be used to provide an action spectrum of the absorption to the S_1 excited state. The (nanosecond) laser wavelength was scanned between 2.0 < *hν* < 2.6 eV (620 > λ > 470 nm) and total electron yield on the imaging detector was monitored. Fig. 4 shows the resulting action spectrum, which has been scaled with the laser pulse energy to compensate for changes in intensity as the wavelength was tuned. Also shown is the absorption spectrum of InC^{2-} in methanol. The overall profile of the action spectrum is very similar to the absorption spectrum for InC^{2-} in solution, providing some confidence that the action spectrum faithfully represents the intrinsic absorption spectrum of InC^{2-}.

Solvation introduces a large red-shift in the $S_1 \leftarrow S_0$ absorption. The intrinsic maximum occurs at λ_{max} = 2.21 eV (560 nm), while in methanol, this is shifted to λ_{max} = 2.07 eV (600 nm), corresponding to a shift of 0.14 eV (40 nm). These observations are comparable to those observed in neutral indigo for which the absorption maximum has been measured to be λ_{max} = 2.27 eV (546 nm) in the gas-phase, relative to λ_{max} = 2.05 eV (605 nm) in methanol (a 0.22 eV shift). [33, 34]

The bathochromic shift of indigo has been attributed to the unique arrangement of the N–H electron donor and C=O electron acceptor groups in the chromophore which has a structure resembling an "H" (see Fig. 1(a)). The LUMO is particularly well stabilised in polar solvents because it exhibits an increased charge separation relative to the HOMO.[35-38] Consequently, the HOMO-LUMO gap is larger in the gas-phase in the absence of the polar stabilisation of the LUMO. The same picture appears valid for the InC^{2-} system although the solvatochromism is perhaps slightly

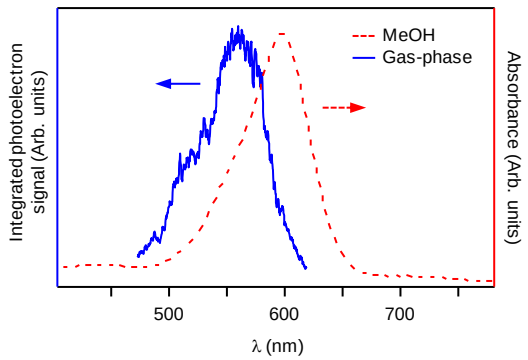

Fig. 4 Action (absorption) spectrum of InC^{2-} in the gas phase (solid line) and absorption spectrum in a methanol solution (dashed line). The gas phase spectrum is similar to the solution-phase absorption spectrum, but blue-shifted by 40 nm.

weaker than for neutral indigo. Nonetheless, it demonstrates that InC^{2-} is an appropriate system to study the photophysics of indigo in the gas-phase. Our choice of InC^{2-} has, however, primarily been motivated because of its more recent use in excited state dynamics studies compared to indigo which is much less readily dissolved (and also more difficult to electrospray).

Time-resolved photoelectron spectroscopy

To determine the intrinsic dynamics of InC^{2-}, time-resolved PE spectroscopy has been employed. A laser pulse centred at the maximum absorption of the $S_1 \leftarrow S_0$ transition (2.21 eV (560 nm)) was used as a pump pulse, while a 3.10 eV (400 nm) probe pulse was used to monitor the excited state population as a function of time-delay, *t*. The PE signal arising only from the 3.10 eV probe is very small compared to the signal from the 2.21 eV pump. At 3.10 eV, the photon energy is no longer resonant with the $S_1 \leftarrow S_0$ transition and is insufficient to directly detach an electron from the system (*i.e.* the RCB is too high – see Fig. 3). The 2.21 eV (560 nm) pump also has insufficient energy to induce direct single photon detachment. However, a relatively strong photoelectron signal is seen between 1 eV < *eKE* < 2 eV. This can be attributed to the resonance-enhanced 2-photon photo-detachment via the S_1 state.

The PE spectrum following 2-photon photodetachment from the pump centred at 2.33 eV (530 nm) is shown in Fig. 5(a), in which the probe arrives before pump pulse, *t* < 0. For comparison purposes, we show the spectrum at 2.33 eV rather than 2.21 eV, as the total energy imparted following two-photon absorption is equal to the 4.66 eV PE spectrum (shown in Fig. 2). Indeed, the two spectra are qualitatively similar. The maximum *eKE* is consistent with the absorption of two-photons at 2.33 eV and the low energy cut-off due to the RCB is identical in both spectra. The bimodal structure in the 4.66 eV PE spectrum is not clearly reproduced in the two-photon spectrum. This may be due to differences in cross section to detachment from the S_1 relative to the S_0 state to the D_0 or D_1 anionic states, or due to the differing Franck-Condon windows accessed. The theoretical work by Yamazaki *et al*. suggests that the S_1 excited state surface is rather flat, which would be consistent with a very broad photoelectron distribution from the S_1 excited state if the final states are not similarly flat.

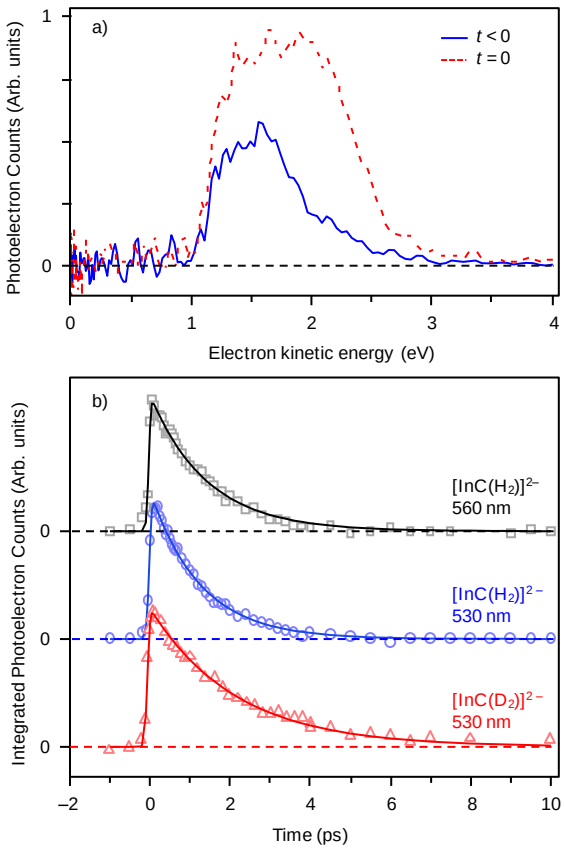

Fig. 5 a) Photoelectron spectra of $[InC(D_2)]^{2-}$ with a 2.33 eV pump and 3.10 eV probe. Solid line represents a typical spectrum in which the probe is arriving before pump, while the dashed line is shortly after t_0. The difference in photoelectron signal is representative of the S_1 excited state population. b) Integrated photoelectron yields of the S_1 excited state signal as a function of time for $[InC(H_2)]^{2-}$ at pump energy of 2.21 eV (560 nm) (squares) and at 2.33 eV (530 nm) for $[InC(H_2)]^{2-}$ (circles) and $[InC(D_2)]^{2-}$ (triangles).

When the pump arrives before the probe, $t > 0$, a considerable increase in PE yield is observed as shown in Fig. 5(a). The enhanced feature is broad, structureless and similar in appearance to the spectrum at $t < 0$, but it extends to higher *eKE*, as expected from the extra energy imparted into the system (an additional 0.77 eV is imparted). As a function of time, the spectral shape of the PE distribution does not change significantly. The only observed change is a decrease in the PE yield as the delay is increased. The pump-probe PE spectra taken with a 2.21 eV pump are qualitatively the same as those taken with the 2.33 eV pump.

In order to determine the kinetics of the excited state dynamics following excitation at the absorption maximum (2.21 eV), the integrated PE signal has been plotted as function of *t*. For this we have taken only the pump-probe signal by subtracting a PE spectrum at $t < 0$ from all other spectra. The total PE yield as a function of time is shown as squares in Fig. 5(b). The kinetics appears first order and the data are well reproduced by a single exponential decay convoluted with the Gaussian instrument response function. The resulting fit is shown by a solid line in Fig. 5(b), from which a lifetime has been deduced to be 1.4 ± 0.2 ps. Following excitation at 2.33 eV (Fig. 5(b), circles), a similar timescale of 1.2 ± 0.2 ps has been obtained. Although this is marginally faster, within our error bounds the timescales are effectively the same.

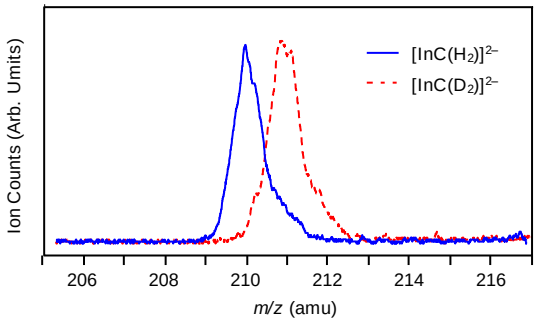

Fig. 6 Mass spectra of $[InC(D_2)]^{2-}$ and $[InC(D_2)]^{2-}$. Complete deuteration is demonstrated by the increase of 1 *m/z* when InC is sprayed from D_2O:acetontrile.

We have also performed time-resolved PE spectroscopy on deuterated InC^{2-}. The H atoms forming the intra-molecular hydrogen bonds can be exchanged for D atoms by dissolving the InC sodium salt in a 20:80 D_2O:acetonitrile solution instead of H_2O:acetonitrile. The effective D exchange is verified by the mass-spectrum as shown in Fig. 6. The mass/charge separation between the two ion peaks is 1 amu, indicating that both H atoms have been exchanged forming the dianionic $[InC(D_2)]^{2-}$ species. The total integrated pump-probe PE signal as a function of time following excitation at 2.33 eV of $[InC(D_2)]^{2-}$ is shown in Fig. 5(b) as triangles and clearly shows that the lifetime is significantly longer. The data are fit to the same function as protonated InC^{2-} and the lifetime extracted is found to be 2.3 ± 0.2 ps, thus giving an isotope effect $\tau_D / \tau_H \sim 2$.

Discussion

Intrinsic decay dynamics

In the absence of solvent, the intrinsic S_1 excited state lifetime is 1.4 ps. This almost doubles when the H atoms involved in intra-molecular hydrogen bonding are replaced with D atoms. The large kinetic isotope effect strongly points to the involvement of the H atoms in the dynamics on the S_1 excited state, confirming that the primary dynamics involves ESIPT. The isotope effect observed in the gas-phase is somewhat larger than in solution, but likely within the combined error of both experiments.[19] The primary process in the gas-phase is the same as in solution, in which the ESIPT can be identified from spectral signatures in the IR and has been shown to be independent on solvent.[17] Hence, it would appear that the ESIPT process in indigo is almost entirely independent of the environment.

The timescale for ESIPT in solution has been determined to be on the order of 600 fs.[18] In our experiment, no wavepacket motion can be discerned in the time-resolved PE spectra and the timescale for this oscillatory motion cannot be directly determined. However, the excited state dynamics calculated by Cui and Thiel point to a similar timescale predicted in vacuum for the ESIPT. These calculations were performed on the bispyrroleindigo derivative of indigo. They find that the ESIPT in the forward direction takes 600 fs. No significant back-reaction is observed in their simulations and the excited state evolves towards internal conversion geometries leading to an average predicted lifetime of 700 fs. This is in fair agreement with our

observations. However, if we assume that the ESIPT for InC^{2-} in vacuum is similar to that in solution – which is justified given that the ESIPT is observed to be independent on solvent – then there is sufficient time for the ESIPT back-reaction to be accessible in vacuum. Yamazaki *et al*. have shown that the potential energy surface for indigo and bispyrroleindigo have important differences.[9] In particular, no barrier to ESIPT is observed for bispyrroleindigo and the lowest conical intersection with the S_0 lies at an energy below the energy associated with the geometry at the Franck-Condon region by about 0.7 eV. In contrast, for indigo, a small 0.2 eV barrier was identified to access the mono-enol from the keto-form. After the mono-enol tautomer is formed, the system can evolve to a conical intersection that has been identified to be ~0.1 eV higher than this barrier. This is consistent with our observations and does indeed suggest that back-ESIPT will be possible on the S_1 state given that the excited state lifetime is 1.4 ps. This is also the case in solution where the S_1 lifetime exceeds the ESIPT process by orders of magnitude. The similarity between kinetic isotope effects suggests that the dynamics of ESIPT are similar in all environments and that the ESIPT motion on the S_1 proceeds via a similarly small barrier.

We point out that double ESIPT cannot be ruled out based on our data alone, but given the comparison with solution phase work, we can dismiss this with some confidence. This is in agreement with the large barrier calculated for this process.[9]

Effect of solvation on S_1 dynamics

Given the similarity between the ESIPT dynamics regardless of the environment, it seems surprising that the S_1 lifetime is affected so strongly by solvation. In solution, the decay of the S_1 state is multi-exponential and highly dependent on the solvent.[20] The slowest component of the decay ranges in lifetime from 2.7 ps in water, to 22 ps in methanol and 92 ps in DMSO, while the fastest component decays in 180 fs for H_2O, and around 500 fs in both methanol and DMSO. Based on the vibrational dynamics, the actual ESIPT mechanism in both protic methanol and aprotic DMSO takes around 600 fs for a full oscillation.[18] The individual timescales are difficult to assign; Franck-Condon factors and selection rules will affect the shape of the decays. In the gas-phase, the decay is mono-exponential. PE spectroscopy, unlike optical methods, does not have stringent selection rules and the probe step (photodetachment) is universally allowed. Hence, it is not unreasonable to consider that Franck-Condon factors and absorption/emission spectral shifts with time are at least partially responsible for the observed complex dynamics in solution. It is tempting to assign the shortest decay observed by Nagasawa *et al*. to the ESIPT process, because for both DMSO and methanol it has a lifetime that is approximately the same as the time for one complete ESIPT cycle (~600 fs). However, given the complex multi-exponential nature of the decays, this assignment cannot be definitive. In particular, it seems unlikely that the time for ESIPT in aqueous solution is just 180 fs, with almost no kinetic isotope effect.[20]

Solvation has the effect of decreasing the rate of internal conversion relative to the gas-phase. Yamazaki *et al*. have briefly discussed solvation effects on the excited state.[9] The keto-form has no dipole moment while the mono-enol does. The effect of solvation will then be to lower the barrier as the mono-enol form is stabilised relative to the keto-tautomer and, hence, the rate of reaction is faster in more polar solvents. Although reasonable, this appears to be in contradiction with our observation that shows that the excited state lifetime is even faster if there is no solvent at all.

The reduced rate of internal conversion in solution points to a higher barrier to access conical intersections relative to the gas-phase. Indigo possess a significant degree of solvatochromism, as evidenced by our gas phase absorption spectrum on InC^{2-}, as well as those on neutral indigo.[34, 36] In the vertical Franck-Condon region (of the keto-tautomer), the excited state is stabilized by 0.14 eV in methanol, however the effect on the mono-enol or conical intersection geometries is not known. Given the significant change in intra-molecular hydrogen bonding when going from the keto to the mono-enol, it is reasonable to expect that the solvent response will be different and for the effect of protic and aprotic solvents to be different. Protic solvents may raise the barrier to the conical intersections relative to the gas phase and aprotic solvents may raise it further. This hypothesis is supported by the findings from temperature dependant fluorescence that the deactivation of InC is a barrier crossing process, and that the barrier is larger in aprotic solvents than protic ones.[20] It is interesting to note that protic solvents tend to distort the structure of InC away from a planar geometry and we speculate that changes in the planarity of the molecule could be influential in modifying the ease with which the conical intersections can be accessed.[20] The conical intersection calculated by Yamazaki *et al.* were performed for indigo in a fixed planar geometry and it would be interesting to see how out-of-plane modes affect the potential energy surface.

One other potential cause for differences between the gas and solution phases is the presence of the two charged sulfate groups. Solvents, and particularly polar ones, will effectively shield the chromophore from these charges, whereas in the gas phase no shielding is present. The perturbation caused by these charges may affect the potential energy surface leading to the observed lifetime changes. However, given the overall similarities in the absorption spectra and primary ESIPT processes, which one might anticipate to be more sensitive to this strong electrostatic interaction, it does not appear that this is the cause.

Conclusions

Using time-resolved photoelectron spectroscopy of the indigo carmine dianion in the gas-phase we have shown that, following excitation to the S_1 excited state, ESIPT is the primary mechanism occurring on the excited state. The ESIPT mechanism appears to be independent of the environment. On the other hand, the overall S_1 lifetime is highly solvent dependant, due to changes in the accessibility of the conical intersection between the S_1 excited state and the S_0 ground state. We have also measured a gas-phase absorption spectrum of InC^{2-}, which echoes neutral indigo well, supporting the suitability of studying it in place of the less soluble neutral indigo. Our data can be compared directly to recent theoretical efforts that have calculated the excited state potential energy surface as well as identified conical intersections that lead to internal conversion. Together, this provides a clear insight into the photo-stability of indigo and its derivatives.

Acknowledgements

This work has been supported by the EPSRC (EP/D073472/1) and by the Leverhulme Trust. We are also grateful to the EPSRC laser loan pool for the loan of the nanosecond laser system.

Notes and references

[a]*Department of Chemistry, University of Durham, South Road, Durham DH1 3LE, United Kingdom.*
[b]*Department of Chemistry, University of Warwick, Gibbet Hill, Coventry CV4 7AL, United Kingdom*
E-mail: j.r.r.verlet@durham.ac.uk; Tel: +44191 3342159

1. G. Carr, *Oxford Journal of Archaeology*, 2005, **24**, 273-292.
2. E. Ferreira, A. Hulme, H. McNab and A. Quye, *Chem. Soc. Rev.*, 2004, **33**.
3. A. Sobolewski and W. Domcke, *J. Phys. Chem. A*, 2001, **105**, 9275-9283.
4. M. N. R. Ashfold, B. Cronin, A. L. Devine, R. N. Dixon and M. G. D. Nix, *Science*, 2006, **312**, 1637-1640.
5. N. Balucani, *International Journal of Molecular Sciences*, 2009, **10**, 2304-2335.
6. J. Seixas de Melo, R. Rondão, H. Burrows, M. Melo, S. Navaratnam, R. Edge and G. Voss, *ChemPhysChem*, 2006, **7**, 2303-2311.
7. J. Seixas de Melo, A. P. Moura and M. J. Melo, *J. Phys. Chem. A*, 2004, **108**, 6975-6981.
8. G. Cui and W. Thiel, *PCCP*, 2012.
9. S. Yamazaki, A. Sobolewski and W. Domcke, *PCCP*, 2011, **13**, 1618-1628.
10. A. Cembran, F. Bernardi, M. Garavelli, L. Gagliardi and G. Orlandi, *J. Am. Chem. Soc.*, 2004, **126**, 3234-3243.
11. G. Zimmerman, L.-Y. Chow and U.-J. Paik, *J. Am. Chem. Soc.*, 1958, **80**, 3528-3531.
12. D. Waldeck, *Chem. Rev.*, 1991, **91**, 415-436.
13. G. Wyman, *Chem. Rev.*, 1955, **55**, 625-657.
14. G. Wyman, *J. Chem. Soc. D*, 1971, 1332-1334.
15. G. Wyman and B. Zarnegar, *J. Phys. Chem*, 1973, **77**, 1204-1207.
16. T. Kobayashi and P. M. Rentzepis, *J. Chem. Phys.*, 1979, **70**, 886-892.
17. I. Iwakura, A. Yabushita and T. Kobayashi, *Bull. Chem. Soc. Jpn.*, 2011, **84**, 164-171.
18. I. Iwakura, A. Yabushita and T. Kobayashi, *Chem. Lett.*, 2009, **38**, 1020-1021.
19. I. Iwakura, A. Yabushita and T. Kobayashi, *Chem. Phys. Lett.*, 2010, **484**, 354-357.
20. Y. Nagasawa, R. Taguri, H. Matsuda, M. Murakami, M. Ohama, T. Okada and H. Miyasaka, *PCCP*, 2004, **6**, 5370-5378.
21. T. Suzuki, *Int. Rev. Phys. Chem.*, 2012, **31**, 265-318.
22. J. Verlet, *Chem. Soc. Rev.*, 2008, **37**, 505-517.
23. A. Stolow, A. Bragg and D. Neumark, *Chem. Rev.*, 2004, **104**, 1719-1758.
24. D. Horke, G. Roberts, J. Lecointre and J. Verlet, *Rev. Sci. Instrum.*, 2012, **83**, 063101.
25. J. Lecointre, G. Roberts, D. Horke and J. Verlet, *J. Phys. Chem. A*, 2010, **114**, 11216-11224.
26. A. Eppink and D. Parker, *Rev. Sci. Instrum.*, 1997, **68**, 3477-3484.
27. G. M. Roberts, J. L. Nixon, J. Lecointre, E. Wrede and J. R. R. Verlet, *Rev. Sci. Instrum.*, 2009, **80**, 053104.
28. D. Horke, A. Chatterley and J. Verlet, *The Journal of Physical Chemistry Letters*, 2012, **3**, 834-838.
29. A. Dreuw and L. Cederbaum, *Chem. Rev.*, 2001, **102**, 181-200.
30. X. Wang and L. Wang, *Annu. Rev. Phys. Chem.*, 2009, **60**, 105-126.
31. D. Horke, A. Chatterley and J. Verlet, *Phys. Rev. Lett.*, 2012, **108**, 083003.
32. M. J. Frisch, G. W. Trucks, H. B. Schlegel, G. E. Scuseria, M. A. Robb, J. R. Cheeseman, G. Scalmani, V. Barone, B. Mennucci, G. A. Petersson, H. Nakatsuji, M. Caricato, X. Li, H. P. Hratchian, A. F. Izmaylov, J. Bloino, G. Zheng, J. L. Sonnenberg, M. Hada, M. Ehara, K. Toyota, R. Fukuda, J. Hasegawa, M. Ishida, T. Nakajima, Y. Honda, O. Kitao, H. Nakai, T. Vreven, J. A. Montgomery, J. E. Peralta, F. Ogliaro, M. Bearpark, J. J. Heyd, E. Brothers, K. N. Kudin, V. N. Staroverov, R. Kobayashi, J. Normand, K. Raghavachari, A. Rendell, J. C. Burant, S. S. Iyengar, J. Tomasi, M. Cossi, N. Rega, J. M. Millam, M. Klene, J. E. Knox, J. B. Cross, V. Bakken, C. Adamo, J. Jaramillo, R. Gomperts, R. E. Stratmann, O. Yazyev, A. J. Austin, R. Cammi, C. Pomelli, J. W. Ochterski, R. L. Martin, K. Morokuma, V. G. Zakrzewski, G. A. Voth, P. Salvador, J. J. Dannenberg, S. Dapprich, A. D. Daniels, Farkas, J. B. Foresman, J. V. Ortiz, J. Cioslowski and D. J. Fox, Wallingford CT, 2009.
33. S. E. Sheppard and P. T. Newsome, *J. Am. Chem. Soc.*, 1942, **64**, 2937-2946.
34. G. Haucke and G. Graness, *Angew. Chem. Int. Ed.*, 1995, **34**, 67-68.
35. D. Jacquemin, J. Preat, V. Wathelet and E. Perpète, *J. Chem. Phys.*, 2006, **124**, 074104.
36. E. Wille and W. Lüttke, *Angew. Chem. Int. Ed.*, 1971, **10**, 803-804.
37. S. Dähne and D. Leupold, *Angew. Chem. Int. Ed.*, 1966, **5**, 984-993.
38. M. Klessinger and W. Luttke, *Tetrahedron*, 1963, **19**, 315-335.